行政院國家科學委員會專題研究計畫　成果報告

多相材料的微結構設計(III)奈米鈦酸鋇多相材料

計畫類別：個別型計畫
計畫編號：NSC92-2216-E-002-029-
執行期間：92 年 08 月 01 日至 93 年 07 月 31 日
執行單位：國立臺灣大學材料科學與工程學研究所

計畫主持人：段維新
共同主持人：楊聰仁
計畫參與人員：張東明博士(博士後研究)，黃永慶，李炤佑，陳盈樺，許秀菁

報告類型：精簡報告
報告附件：出席國際會議研究心得報告及發表論文
處理方式：本計畫可公開查詢

中　華　民　國 93 年 10 月 8 日

行政院國家科學委員會專題研究計畫成果報告

多相材料的微結構設計(三) 納米鈦酸鋇多相材料

Microstructural Design of Multiphased Materials (II) Multiphased $BaTiO_3$-matrix Nanocomposites

計畫編號：NSC92-2216-E-002-029
執行期限：92年8 月1 日 至93年7 月31 日

主持人: 段維新 教授
共同主持人: 楊聰仁 教授
執行機構: 國立台灣大學材料科學及工程學研究所
計畫參與人員: 張東明博士(博士後研究), 黃永慶, 李炤佑, 陳盈樺, 許秀菁

I. 摘要

目前金屬鎳已常被使用為高容值積層陶瓷電容 (MLCC)的內電極，且為了提升體積效率，金屬鎳顆粒已由微米級尺寸降至奈米級尺寸．本研究探討鈦酸鋇/鎳奈米多相材料的製備及微結構的關連，研究結果顯示此奈米多相材料可以1330C以上的溫度及低氧分壓的氣分中，以無壓燒結法製備，在此條件下1000± 100 ppm 的鎳可溶入鈦酸鋇中，而鎳的擴散距離可達10□m．鎳溶質的存在可大幅減少鈦酸鋇不正常晶粒的產生．但鎳溶質及鎳顆粒皆會大幅降低緻密化及晶粒成長速率．

Abstract

Nickel is now used as the internal electrode for the multilayer ceramic capacitors (MLCCs). In order to increase its volume efficiency, the size of Ni particles decreases from micrometer-sized range to nanometer-sized range. In the present study, nano-sized Ni particles are mixed intimately with $BaTiO_3$ powder. The powder compacts are then co-fired in an atmosphere with low oxygen partial pressure. The sintering behavior of the Ni-doped $BaTiO_3$ is investigated. The presence of the nanometer-sized Ni inclusions can inhibit the grain growth of $BaTiO_3$. The solubility of Ni in $BaTiO_3$ during co-firing is also determined. Two techniques have been applied to determine the solubility. Consistent results are obtained. The solubility of the Ni in the $BaTiO_3$ is around 1000±100 ppm after co-firing at 1330°C for 2 h in N_2.

II. Introduction and Objectives

Barium titanate ceramics are widely used as dielectric in capacitor due to its high relative permittivity. The capacitance is further enhanced by utilized multilayered structure. The technology for MLCCs mainly involves the co-firing of dielectrics and electrode materials. Nickel is now utilized as the inner electrode in the $BaTiO_3$-based MLCCs due to its higher melting point [1-4]. However, the Ni electode is easily oxidized during sintering in air. Consequently, a low oxygen partial pressure $P(O_2)$ during firing is necessary. Unfortunately, $BaTiO_3$ is reduced and becomes semiconductor if the Po_2 is too low. It is thus very important to prevent the semiconducting of $BaTiO_3$ as it is sintered in low partial pressure $P(O_2)$. The process condition must be carefully controlled to obtain $BaTiO_3$ insulator with Ni conductor [5-8]. In present study, the effects of nano-size Ni additions on the sintering behaviour and microstructure of $BaTiO_3$ materials are examined.

III. Experimental

Barium titanate powder (NEB, Product No. 52909, Ferro Co., USA) and various amount of nickel nitrate (ACROS Organics Co., USA) were tumble milled together in ethyl alcohol for 4 h. The Ba/Ti ratio of the $BaTiO_3$ powder is 1.000±0.002 as reported by the manufacturer. The grinding media used was zirconia balls. The slurry was dried using by a rotary

evaporator. The dried lumps were then crushed and passed through a plastic sieve. The powder was calcined in air at 500℃ for 2 h and sieved again. The powder was formed into disks by pressing uni-axially at 25 MPa. The size of the discs is 10 mm in diameter and about 3 mm in thickness. The specimens were then pre-sintered at 800 ℃ for 2 h in a 95%N_2/ 5%H_2 atmosphere in order to reduce the NiO to the nano-size Ni particles. Sintering was then performed in N_2 at 1330℃ for 2 h in a tube furnace. The heating and cooling rates were 3℃/min.

The amount of nickel was determined by using the inductive couple plasma-mass spectrometer (ICP-MS). Shrinkage kinetics were determined by a thermal mechanical analyzer (TMA). Phase identification was performed by using X-ray diffractometry (XRD). The final density was determined by using the water displacement method. The microstructure was observed by scanning electron microscopy (SEM). The electron probe microanalysis (EPMA) was used to determine the solubility of the nickel in the $BaTiO_3$.

IV. Results and Discussion

Fig. 1(a) shows the XRD patterns of the Ni-doped $BaTiO_3$. The amount of Ni in the reduced 1 vol% Ni doped $BaTiO_3$ powder, as revealed by ICP-MS analysis, was 1.33 wt% (～1 vol%). It suggested that there was no loss of Ni during the reduction step. The XRD analysis indicates that a small amount of NiO is present in Ni-doped $BaTiO_3$ specimen in Fig.1(b). It indicates that Ni is partially oxidized during sintering. By using the slow scanning rate and the Scherre's equation, the size of Ni particles can be determined. In the 5 vol% Ni doped $BaTiO_3$ specimen, the size of Ni particles is 70 nm. For the specimens with lower Ni contents, the size of Ni particles should be smaller than this values.

Typical microstructures of the sintered the Ni-doped $BaTiO_3$ specimens are shown in Fig. 2. The size of $BaTiO_3$ grains, especially the size of abnormal grains, depends strongly on the nickel content. The size and the amount of abnormal grains reach their highest values as the nickel content is 0.05 vol%.

The densification curves of the $BaTiO_3$ and the nickel-doped $BaTiO_3$ specimens are shown in Fig. 3. The density of Ni-doped $BaTiO_3$ is lower than that of pure $BaTiO_3$ in terms of the same temperature, Fig. 3(a). It is due to that the densification rate of $BaTiO_3$ is significantly reduced because the addition of nano-sized Ni particles, Fig. 3(b). It indicates that Ni ion may dissolve into $BaTiO_3$ to affect its defect concentration, subsequently, its sintering kinetics [10]. The solubility limit obtained in the present study is lower than the values reported by others [5-7,9,11-12]. The discrepancy may result from the different raw material used. When the coordination number is 6, the ionic radius of the Ti^{4+} and Ni^{2+} is 0.61 and 0.69 Å , respectively. The ionic radius of Ba^{2+} ion is 1.59 Å as the coordination number is 12. Although the valence of Ni ion is the same as that of Ba ion, the ionic radius of Ni^{2+} is much smaller than that of Ba^{2+}. The Ni^{2+} is more likely to replace the Ti^{4+} for their similar ionic size [13]. It suggests that Ni ion acts as electron acceptor in $BaTiO_3$ lattice. The replacement of Ti^{4+} by Ni^{2+} is accompanied by the formation of oxygen vacancy as [14]

$$NiO \xrightarrow{BaTiO_3} Ni_{Ti}^{''} + V_O^{\bullet\bullet} + O_O$$

The $BaTiO_3$ crystal is distorted due to the solution of Ni. The fraction of the increase in a-axis is higher than that in c-axis, Fig. 4. The c/a ratio is decreased as Ni content is increased. As the Ni content is higher than a certain value, the value of c/a ratio is stabilized. The solubility of Ni in $BaTiO_3$ crystal can be determined by using Fig. 4. The solubility of Ni in $BaTiO_3$ is about 0.075 vol% Ni.

The solubility of Ni in $BaTiO_3$ crystal has also been determined by using

the EPMA technique as developed by shih and Tuan [15]. Fig.5 displays the line scan result on the solubility of Ni-doped $BaTiO_3$ specimen, which indicates of the solubility is around 1000±100 ppm. The EPMA technique can also provide an idea on the diffusion distance of the nickel into the $BaTiO_3$. Because EPMA always starts from a metallic particle, the signal is high at that point, then drops to a saturated plateau in which solubility can be determined. If the plateau then drops to zero, then the diffusion distance can be determined. An example is shown in Fig. 5. However, if many nickel particles are located near the surface region, or if nickel ions diffuse for a long distance, it is impossible to determine a precise diffusion distance. A lower bound for the diffusion distance then is estimated instead. According to the present EPMA results, the diffusion distance of the nickel into the $BaTiO_3$ was >10 m for the Ni-doped $BaTiO_3$ specimens.

V. Conclusions

1. A small amount of nickel solute can decrease the size of abnormal grains.
2. The Ni addition can also reduce the densification rate and relative density.
3. The solubility of Ni in $BaTiO_3$ 0.075 vol% by using the XRD analysis.
4. Using EPMA technique, the solubility of Ni in $BaTiO_3$ is 1000 ±100 ppm and the diffusion distance of the Ni into the $BaTiO_3$ is >10 m.

REFERENCES

1. H. Kishi, Y. Mizuno and H. Chazono, Jpn. J. Appl. Phys., **42**, 1–15, (2003).
2. I-N Lin, W-C Yang and C-T Hu, J. Am. Ceram. Soc., **64,** 851-858 (2004).
3. Y. Wang, L. Li & J. Qi et al, Materials Science and Engineering, **B99** 378-381 (2003).
4. Y. Sakabe, Am. Ceram. Soc. Bull., **66**, 1338-41 (1987).
5. H. J. Hwang, M. Toriyama, T. Sekino and K. Niihara, J. Eur. ceram. Soc., **18**, 2193-2199 (1998).
6. H. Hyuga, Y. Hayashi, T. Sekino and K. Niihara, NanoStructure Materials, **9,** 547-550 (1997).
7. W. H. Tzing and W. H. Tuan, Ceram. Int. **25,** 69-75 (1999).
8. W. H. Tzing , W. H. Tuan and H. L. Lin, Ceram. Int**. 25,** 452-430 (1999).
9. H. Emoto, and J. Hojo., J. of Ceram. Soc. Jpn. Int. Ed., **100,** 553-7 (1992).
10. C. Y. Chen and W. H. Tuan, J. Am. Ceram. Soc., **83[12]** 2988-92 (2000).
11. H. Ihrig, J. Phys. C: Solid State Phys. **11,** 819-287 (1978).
12. P. Baxter, N.J. Hellicar, B. Lewis, J. Am. Ceram. Soc. **42,** 465-470 (1959).
13. W.H. Tzing and W.H. Tuan, Euro Ceramics V, pp. 1167-70 (1997).
14. H.-J. Hagemann, D. Hennings, J. Am. Ceram. Soc. **64**, 590-594 (1981).
15. S-J Shih and W.H. Tuan, J. Am. Ceram. Soc., **87,** 401-407 (2004).

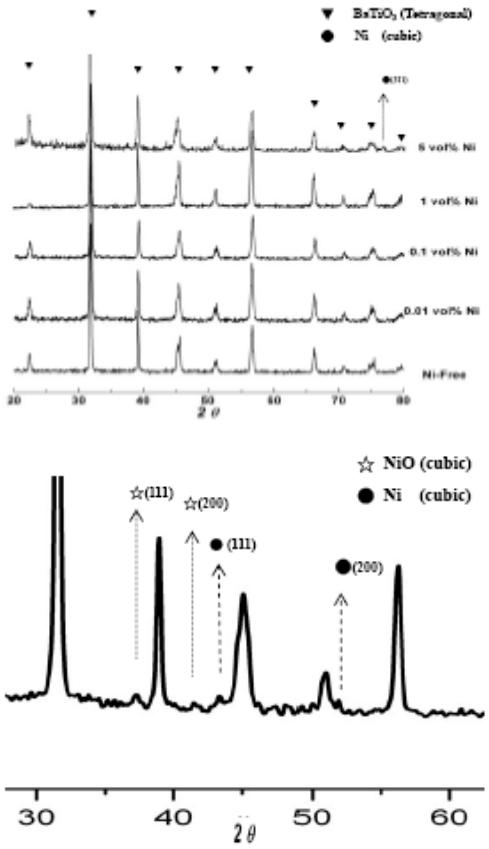

Fig. 1, (a) XRD patterns of the Ni-doped $BaTiO_3$ specimens. (b) A small amount of Ni is dissolved in the $BaTiO_3$.

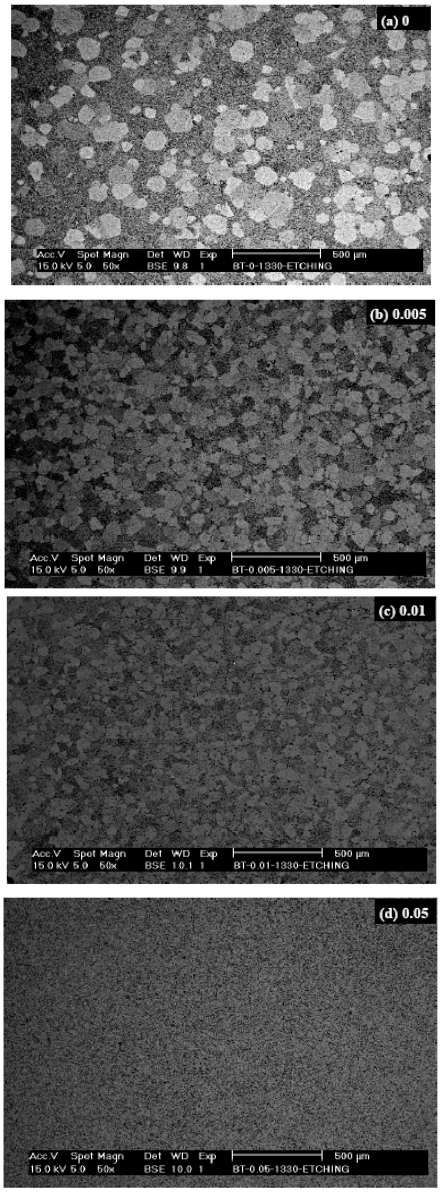

Fig. 2, Typical microstructures of (a) $BaTiO_3$ and (b) 0.005, (c) 0.01, (d) 0.05 vol.% Ni-doped $BaTiO_3$ specimens.

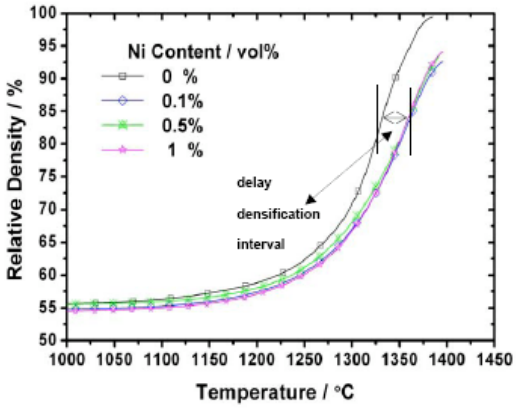

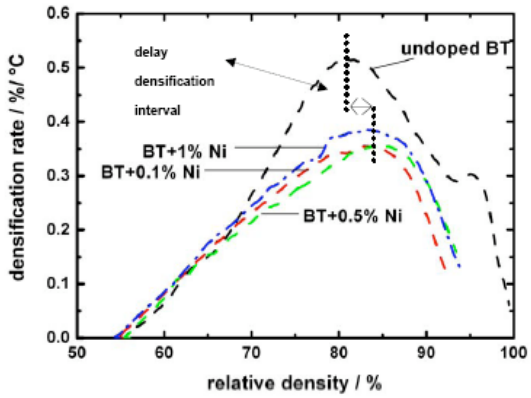

Fig. 3, The sintering kinetics of Ni-doped $BaTiO_3$ specimens.

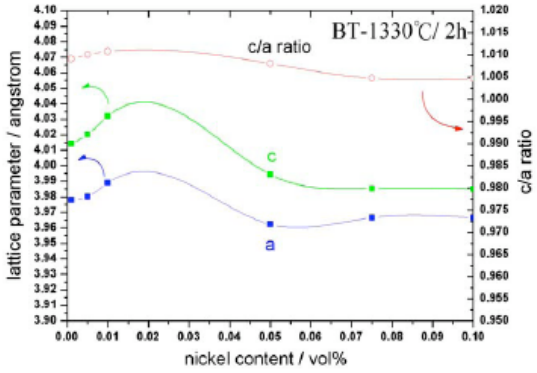

Fig. 4, The c, a and c/a ratio as function of Ni content.

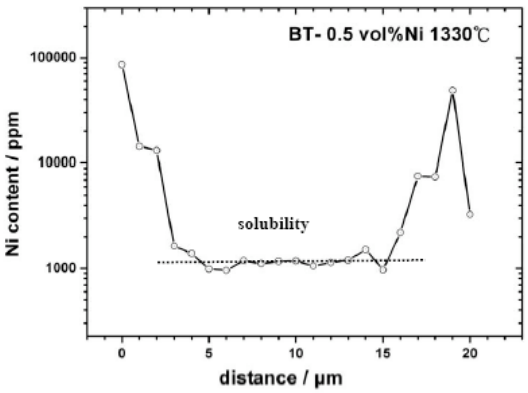

Fig. 5, A typical EPMA curve for a 0.5% Ni-doped $BaTiO_3$ specimen.